Biomaterials 31 (2010) 3762–3771

Contents lists available at ScienceDirect

Biomaterials

journal homepage: www.elsevier.com/locate/biomaterials

Neuronal adhesion and differentiation driven by nanoscale surface free-energy gradients

Guillaume Lamour [a,b], Ali Eftekhari-Bafrooei [b], Eric Borguet [b], Sylvie Souès [c], Ahmed Hamraoui [a,d,*]

[a] Neuro-Physique Cellulaire, Université Paris Descartes, UFR Biomédicale, 45 Rue des Saints-Pères, 75006 Paris, France
[b] Department of Chemistry, Temple University, Philadelphia, Pennsylvania, PA 19122, USA
[c] Régulation de la Transcription et Maladies Génétiques, CNRS UPR2228, Université Paris Descartes, UFR Biomédicale, 45 Rue des Saints-Pères, 75006 Paris, France
[d] Service de Physique et Chimie des Surfaces et Interfaces, CEA Saclay, 91191 Gif-sur-Yvette, France

ARTICLE INFO

Article history:
Received 16 December 2009
Accepted 15 January 2010
Available online 10 February 2010

Keywords:
PC12 cells
Neuronal differentiation
Cell adhesion
Self-assembled monolayers (SAMs)
Sum-frequency generation (SFG)
Surface energy

ABSTRACT

Recent results indicate that, in addition to chemical, spatial and mechanical cues, substrate physical cues such as gradients in surface energy may also impact cell functions, such as neuronal differentiation of PC12 cells. However, it remains to be determined what surface effect is the most critical in triggering PC12 cell differentiation. Here we show that, beyond continuously probing the surface energy landscape of their environment, PC12 cells are highly sensitive to nanoscale chemical heterogeneities. Self-assembled monolayers of alkylsiloxanes on glass were used as a culture substrate. By changing the structure, ordering and chemical nature of the monolayer, the surface energy distribution is altered. While both well-ordered CH_3 terminated substrates and bare glass (OH terminated) substrates did not favor PC12 cell adhesion, PC12 cells seeded on highly disordered CH_3/OH substrates underwent enhanced adhesion and prompt neuritogenesis by 48 h of culture, without nerve growth factor treatment. These data illustrate that surface free-energy gradients, generated by nanoscale chemical heterogeneities, are critical to biological processes such as nerve regeneration on biomaterials.

1. Introduction

Neuronal differentiation is critical to nervous tissue regeneration after injury, and adhesion on a substrate is critical for neurite extension [1–3]. The initiation and guidance of a neurite rely on extra-cellular signals, such as substrate energy of adhesion (e.g., surface energy, or surface tension) [4], especially local gradients [5]. Hence, it is of great interest to unveil the substrates characteristics that are effectively sensed by the growth cone, and translated into neuritis extension as a response to these physical cues. The ability to spatially control the distribution of the energy of adhesion is of particular interest in many biomedical and tissue-engineering applications.

The interactions of cells, especially neurons, with nanoscale topography [6–9], and with surface chemistry [10–12], were reported to be important parameters in controlling cell function. Another parameter, substrate compliance, influences both neuritogenesis [13–16] and neurite branching rate [17]. Thus, a combination of spatial, chemical and mechanical inputs, together with the genetic program of the cell, has been recently proposed to control the shape and functions of cells, as well as of tissues [18]. However the exact role of the surface tension and its spatial variation is still unclear and a systematic study may lead to a better understanding of the surface adhesion parameters that drive neuritogenesis.

Self-assembled monolayers (SAMs) are surface-active materials with many potential applications in biotechnology [19,20]. SAMs of alkylsiloxanes on glass can exhibit a wide range of properties, including the chemical nature, the surface roughness, and the organization of surface-exposed terminal groups. These combined properties generate, at the nanoscale level, distinct surface energy distributions, and at larger scale, macroscopic surface characteristics such as wettability. SAMs of alkylsiloxanes on glass [21,22] or on titanium [23] have been shown to be suitable substrates for controlling cell adhesion, and in particular for controlling neuronal cell differentiation [10,21,23].

PC12 cells, though not primary neuronal cells, express the transmembrane TrkA and p75 receptors to nerve growth factor (NGF) [24,25], and differentiate into a neuronal phenotype when challenged by appropriate NGF concentrations [26]. This ability makes them a well-defined model to study neuronal differentiation mechanisms, and thus axonal regeneration. Several key inducers of PC12 cell neuronal differentiation in NGF-free medium have been identified: PC12 cell neuritogenesis is observed on soft substrates

* Corresponding author. Fax: +33 (0)14 286 2085.
E-mail address: ahmed.hamraoui@parisdescartes.fr (A. Hamraoui).

0142-9612/$ – see front matter © 2010 Elsevier Ltd. All rights reserved.
doi:10.1016/j.biomaterials.2010.01.099

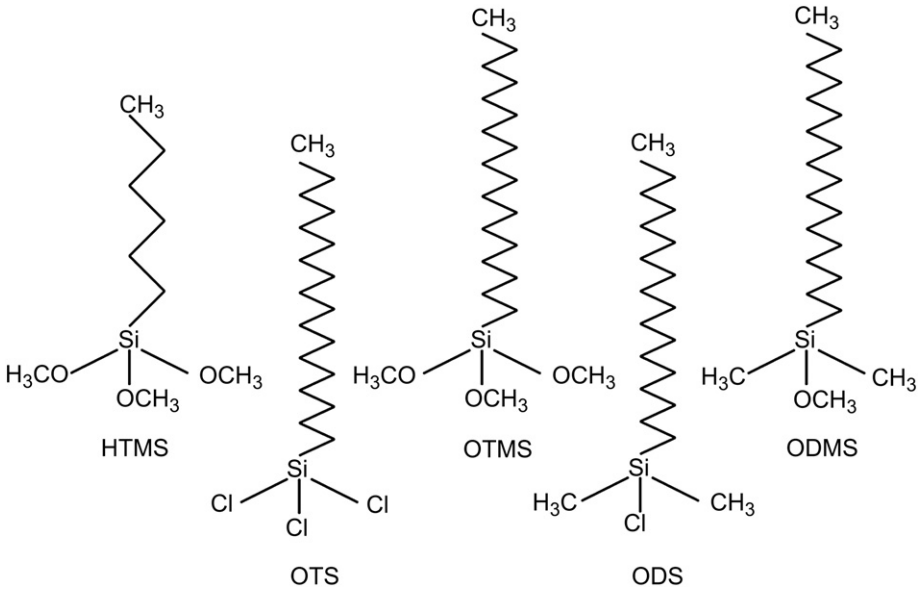

Fig. 1. Schematics of methyl-terminated molecules used to modify glass surfaces. Molecules were grafted onto clean glass surfaces by chemisorption from the liquid phase. HTMS, OTMS and OTS cross-link during SAMs formation, contrary to ODMS or ODS, that can bind glass surfaces through only one bond, following hydrolysis of their unique OCH_3 or chlorine leaving group.

composed of extra-cellular matrix (ECM) proteins such as collagen, fibronectin and laminin [27], or of ECM derived from astrocytes [28].

In our previous study [5], we demonstrated the differentiation ability of PC12 cells in NGF-free medium when seeded on solid glass substrates covered with NH_2-terminated alkylsiloxane SAMs. These surfaces contained a nanoscale mixture of hydroxyl and amine groups which provided local gradients in surface energy. However, we did not determine whether the trigger of PC12 cell differentiation was the surface nanoroughness, the surface concentration in terminal amines, the alternation of OH and NH_2 groups, or a combination of these factors.

Here we examined the influence of these potential triggers, again by tailoring various silanes on glass [29], which provide cell culture substrates. We used methyl-terminated silanes that offer two main advantages compared to aminosilanes. First, because of the smaller reactivity of CH_3 compared to NH_2 groups, the control over adsorption process is easier. It is noted that the highly reactive leaving groups of silanes molecules (chlorine and methoxy) react with the silanol groups and/or adsorbed water on the glass surface and are present on the side of the molecule close to the glass surface, away from CH_3 terminal groups (Fig. 1). Second, vibrational spectroscopy which is used for the surface characterization is more reliable in the CH stretching region (2800–3000 cm^{-1}) than in the NH stretching region (3100–3500 cm^{-1}) where the broad OH vibrational spectrum of adsorbed water smears out the NH peaks. Furthermore, CH groups do not provide polar component to the surface free energy (SFE), thus facilitating the SFE calculations and SFE analysis.

2. Materials and methods

2.1. Chemicals

Chemicals were obtained from Acros Organics (Geel, Belgium), Sigma–Aldrich (St. Quentin Fallavier, France), ABCR (Karlsruhe, Germany), Fisher Scientific (Illkirch, France) and Carlo Erba Reagents (Val de Reuil, France). The sources and purity of the chemicals used are summarized in Table 1.

2.2. Substrates preparation

Modified glass slides (SuperFrost®, 25 × 75 × 1 mm^3, Menzel-Glaser, Braunschweig, Germany) were used for optical studies, and modified glass coverslips (30-mm diameter and 100-μm thick, Menzel-Glaser) were used for cell culture experiments. Prior to use, glassware was cleaned by immersion in piranha solution (3:1 (v/v) sulfuric acid:40% hydrogen peroxide), then thoroughly rinsed with deionized water and dried under a nitrogen stream (*caution: piranha solution is extremely corrosive and can react violently with organic compounds. Appropriate safety precautions including gloves and face shield should be used when handling.*). Glass coverslips were cleaned by immersion in ultrasonic bath of chloroform for 20 min prior to immersion in piranha solution. For the self-assembly, the cleaned glass substrates were immersed into solutions (Table 2) of the desired alkylsilanes (Fig. 1). The chemically modified substrates were then rinsed with the neat solvent. Prior to cell culture, the substrates were dried under a laminar flow hood and prior to surface characterization, the substrates were dried under a nitrogen stream. All treatments were carried out at room temperature and in ambient atmosphere (relative humidity ≈ 50%).

2.3. Surface characterization

2.3.1. Fourier transform infrared spectroscopy

Fourier transform infrared spectroscopy (FTIR) spectra were measured in the transmission geometry at a normal incidence angle using a Bruker Optics TENSOR 27

Table 1
Chemicals used for surface modification and contact angle measurements.

	Manufacturer	Purity (%)
Deionized water (Elga UHQ PS MK3)	Veolia Water Systems	(ρ = 18.2 MΩ.cm)
Hexanes (HX) (mixture of isomers)	Sigma–Aldrich	≥98.5 (ACS)[a]
Methanol (MET)	Carlo Erba Reagents	>99.9 (HPLC)[a]
Acetic acid (AA)	Carlo Erba Reagents	99.9 (RPE)
Sulfuric acid	Sigma–Aldrich	95–97
Hydrogen peroxide	Sigma–Aldrich	40 (m/v in H_2O)
Chloroform (CF)	Carlo Erba Reagents	>99.8 (ACS)
n-Hexyltrimethoxysilane (HTMS)	ABCR	97
n-Octadecyltrimethoxysilane (OTMS)	Acros Organics	95
Octadecyldimethylmethoxysilane (ODMS)	ABCR	95
n-Octadecyltrichlorosilane (OTS)	Acros Organics	95
Octadecyldimethylchlorosilane (ODS)	Sigma–Aldrich	95
Glycerol (GL)	Acros Organics	≥99
Formamide (FA)	Fisher Scientific	≥99.5
n-Hexadecane (HD)	Acros Organics	99
Tetradecane (TD)	Sigma–Aldrich	≥99
n-Dodecane	Fisher Scientific	>98
n-Undecane	Acros Organics	99
n-Octane	Acros Organics	95

[a] Water content is <0.01% (v/v).

Table 2
Description of the chemical processes used to modify glassware. The abbreviations in capital letters refer to the chemicals displayed in Table 1.

Substrate	Solution	Adsorption time	Rinsing solvent(s)	Note(s)
ots	0.1% OTS + 20% CF + 80% HD	15 min	CF and MET	[a]
ods	0.1% ODS + 20% CF + 80% HD	15 min	CF and MET	[a,b]
otms	1% OTMS + 99% HX	4 h	HX and MET	
$otms_x$	1% OTMS + 99% HX	4 h	HX and MET	[a]
$odms_1$	1% ODMS + 99% HX	~10 h	HX and MET	[a]
$odms_2$	1% ODMS + 99% HX	>24 h	HX and MET	
$htms_{M1}$	2% HTMS + 94% MET + 4% H_2O + 1 mM AA	~16 h	MET	
$htms_{M2}$	2% HTMS + 94% MET + 4% H_2O + 1 mM AA	~24 h	MET	
$htms_{M3}$	2% HTMS + 94% MET + 4% H_2O + 1 mM AA	>72 h	MET	
$htms_H$	1% HTMS + 99% HX	4 h	HX and MET	
$htms_{Hx}$	1% HTMS + 99% HX	4 h	HX and MET	[a]

[a] Solution was slowly agitated with a rotating magnet all along the reaction.
[b] ODS was slightly heated until it reached a liquid phase (at 28–30 °C), just before being added to the solvent solution.

spectrometer equipped with a DTGS detector. FTIR spectra were background corrected by subtraction of a spectrum of the clean, bare substrate (e.g., SAM-free), and recorded by integrating 200 scans with a resolution of 4 cm^{-1}.

2.3.2. Vibrational sum-frequency generation

Sum-frequency generation (SFG) is a surface vibrational spectroscopy based on a second-order non-linear optical process in which two laser beams with frequencies ω_1 and ω_2 overlap on the surface and generate a coherent response whose frequency is the sum of two incident laser ($\omega_{SFG} = \omega_1 + \omega_2$). In the electric dipole approximation, second-order non-linear optical processes, including SFG, do not take place in media with inversion symmetry but do occur at interfaces as the inversion symmetry is necessarily broken there. Therefore, by selecting one of the incident beams to be in the IR region ($\omega_1 = \omega_{IR}$) and the other in the visible region ($\omega_2 = \omega_{vis.}$), SFG can be used as a powerful spectroscopic technique to measure surface vibrational spectra [30]. A detailed description of our SFG set up can be found elsewhere [31]. Briefly, IR and visible pulses with energies of 15 and 2 μJ, incident at the surface with the angles of 72° and 65° respectively, were focused to beam waists of 250 and 200 μm, respectively. The SFG signal was detected with a CCD (Princeton Instrument) coupled with a spectrograph (300i, Acton Research Corp.). The polarization of visible and SFG were controlled by a combination of polarizers and half-wave plates. In the experiments presented here, the polarization combination of SFG, visible, and IR were either S,S,P or P,P,P.

2.3.3. Contact angle measurements

Contact angles (θ) were measured as described in Ref. [5]. Briefly, an image of the profile of a drop on a solid surface was recorded using a CCD video camera (Sony DXC-101P). The image was then processed with ImageJ software (Wayne Rasband, National Institutes of Health, Bethesda, MD) using the Contact Angle plug-in (Marco Brugnara, University of Trento, Trento, Italy), which calculates the contact angle value from the profile of the drop. At least 3 drops per sample were analyzed.

2.3.4. Determination of surface free energy

The surface free energies (SFE) of samples were calculated using the Owens–Wendt theoretical model [32]. This model gives the long-range dispersion (Lifshitz–Van der Waals; γ^d) and the short-range polar (hydrogen bonding; γ^p) components of SFE according to the following equation:

$$W_{SL} = (1 + \cos\theta)\gamma_L = 2\left(\gamma_s^d\right)^{1/2}\left(\gamma_L^d\right)^{1/2} + 2\left(\gamma_s^p\right)^{1/2}\left(\gamma_L^p\right)^{1/2} \quad (1)$$

where γ_s is the SFE of the surface, γ_L is the SFE of the liquid and W_{SL} is the solid–liquid interface energy. Two liquids were used as probes for SFE calculations: n-hexadecane, and H_2O. For a liquid, the overall surface tension (γ_L) is a combination of dispersive and polar components, whose values are indicated in Table 3 (adapted from Ref. [33]). The contact angles of n-hexadecane and H_2O were reported in Eq. (1) for each solid substrate, then sample SFE components were calculated.

The critical surface tension γ_c was calculated using the Fox–Zisman approximation. In this work, it can be understood as a first-order approximation of the Good–Girifalco equation [35], for a surface tension of the liquid γ_L ($\gamma_L \geq \gamma_c$) close to the γ_c of the solid. Using a linear regression analysis, Zisman plots, $\cos\theta = f(\gamma)$, were traced for each substrate by fitting the data obtained with the test liquids. γ_c values were read where the line fits intersect $\cos\theta = 1$, as described by Zisman [34].

Table 3
Values of the surface tension (γ, mN m^{-1}) of some test liquids at 20 °C (adapted from Ref. [33]). γ^d and γ^p are respectively the dispersive and the polar components of the surface tension.

Liquid	γ	γ^d	γ^p
Water	72.8	21.8	51
Glycerol	64	34	30
Formamide	58	39	19
n-Hexadecane	27.47	27.47	~0
Tetradecane	26.56	26.56	~0

2.3.5. AFM imaging

Each substrate was analyzed using a Bioscope™ AFM (Digital Instruments/Veeco) in air using tapping mode (RTESP tip cantilever, spring constant: 40 N m^{-1}). The root-mean-square (rms) roughness of the surfaces was evaluated for regions of ~1 μm × 1 μm, by AFM software Nanoscope (Veeco). The line scanning frequency was ~0.5 Hz (256 scan lines × 512 pixels). The images were flattened using Nanoscope software before the rms was evaluated.

2.4. PC12 cell manipulation

Unless otherwise specified, the biological products in this section were purchased from Invitrogen (Fisher Bioblock Scientific, Illkirch, France).

2.4.1. Cell culture

PC12 cells (ATCC, CRL 1721) were maintained in Dulbecco's Modified Eagle Medium containing horse serum (5%), fetal calf serum (5%, HyClone), non-essential amino acids (1%) and antibiotics (1%). In the experiments, PC12 cells (passage numbers 7–17) were seeded onto modified glass coverslips, that had been sterilized by immersion in a solution of 70% methanol and 30% H_2O for 15 min. Cells were seeded in a small volume of the culture medium ($V = 335$ μL), in order to trap PC12 cells on the top of the modified substrates. The cell density at the time of seeding was ~10^4 cm^{-2}. Experiments never exceeded 48 h. No further addition of culture medium was made and, in particular, no NGF was added to the culture medium.

2.4.2. Quantification of neuritogenesis

The propensity of PC12 cells to initiate neurites was evaluated on each substrate. At least 10 pictures ($S = 0.182$ mm^2/picture) of the cells cultured on each substrate were taken with a camera mounted on a phase-contrast microscope (Nikon Eclipse TS100), using a ×20 objective. In order to avoid confusing neurites with cell soma protrusions or filopodia, only neurites with length greater than 25 μm were counted. This threshold length corresponds to approximately the diameter of a PC12 cell soma multiplied by 1.5.

2.4.3. Immunofluorescence

PC12 cells were cultured on each substrate, as described above. After 48 h of culture, cells were fixed with 3.7% formaldehyde in PBS for 15 min and then permeabilized with 0.1% Triton X-100 in PBS/0.1% bovine serum albumin (BSA) for 20 min. All washes, blocking steps, and antibody dilutions were performed using 0.1% BSA, 0.01% Triton® X-100 in PBS. After cell fixation and permeabilization, the primary antibody anti-MAP1B (Sigma–Aldrich; diluted 1:800) was incubated overnight at 4 °C. A secondary Cy3-conjugated antibody (Jackson ImmunoResearch, Cambridgeshire, UK; diluted 1:400) was incubated for 2 h at room temperature. DNA was stained with 4-6-diamidino-2-phenylindole (DAPI) at 0.5 g/mL for 15 min. F-actin was stained with phalloidin coupled to Alexa Fluor 488 (Molecular Probes) at 5 units/mL for 30 min. Finally cells were extensively washed in PBS and mounted in a Fluoromount G™ solution (Southern Biotech). Cell observation was done with a Nikon Eclipse E600 epifluorescence microscope coupled to a high resolution colour camera (Nikon DXM 1200), using ×10 and ×50 objectives. No threshold processing was applied to the images.

3. Results and discussion

Molecules (noted in capital letters) of various chain lengths and chemical nature (Fig. 1) were chosen to generate distinct surfaces (noted in small letters), according to their mechanism of adsorption and monolayer formation on glass. The resulting substrates were divided into three different classes (Fig. 2) with regard to nanoscale surface organization and hence to distribution of surface energy. Class 1 SAMs are well-ordered with an all-trans conformation of the alkyl chains. Class 2 SAMs, while eliminating multilayer formation due to the impossibility of the monomers undergoing cross-linking, are disordered. Moreover,

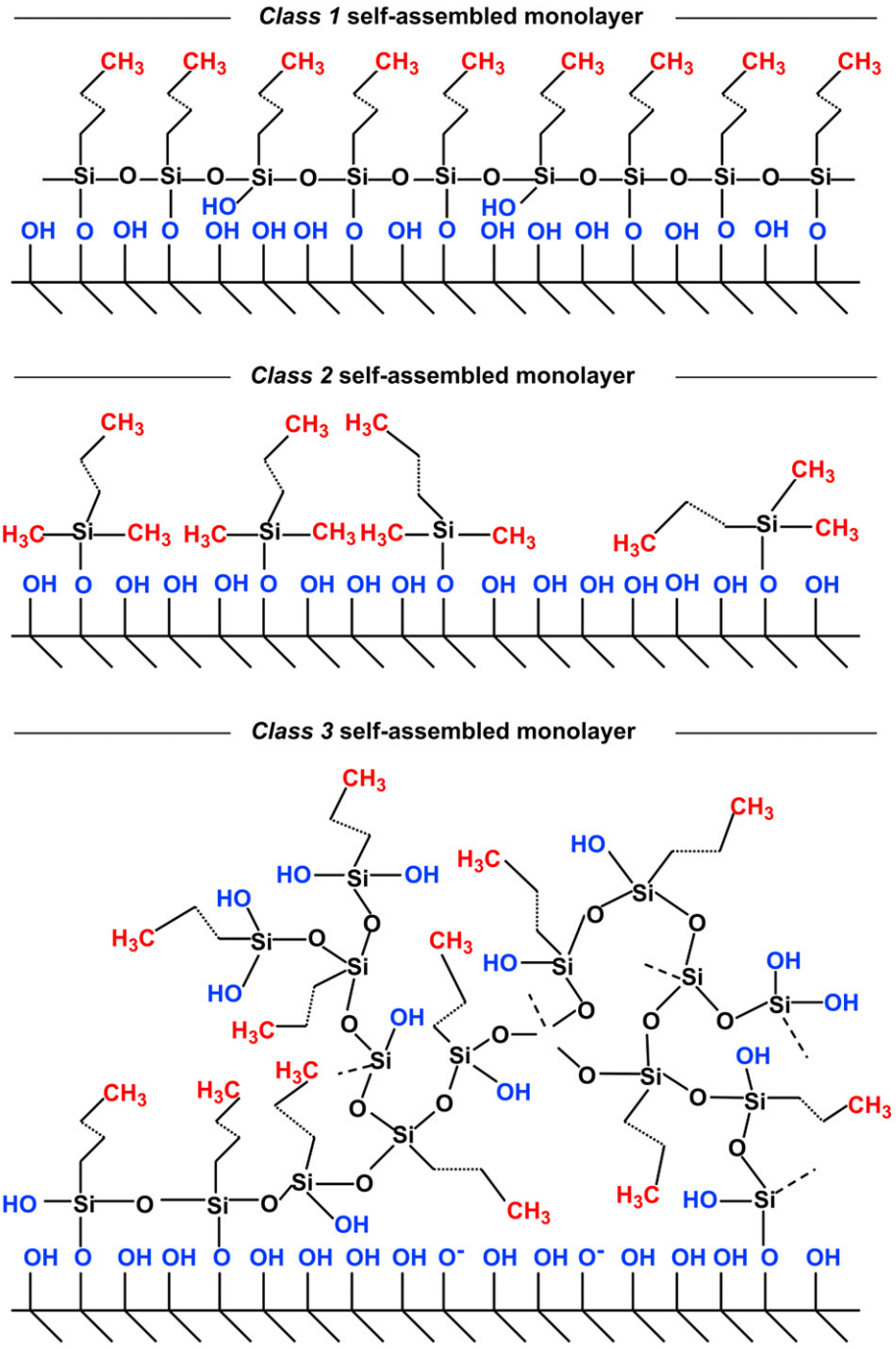

Fig. 2. Sketches representing three distinct organizations of SAMs used as substrates for PC12 cell culture. Class 1 SAMs are well-ordered with an all-trans conformation of alkyl chains. Class 2 SAMs are disordered but limited to monolayer formation. Class 3 SAMs are highly disordered, with possible multilayer formation and higher chemical heterogeneity.

class 2 SAMs likely are accompanied by a significant density of substrate silanol groups (Si–OH), compared to class 1 SAMs. This is a consequence of class 2 monolayer adsorption being incomplete by nature. Class 3 SAMs are the result of chaotic polymerization of a trialkoxysilane. The chemisorption of siloxanes is believed to require activation of the siloxane whereby the leaving group (e.g., OCH_3 in HTMS) is replaced by OH from water. When the solvent solution contains more than the trace amount of water necessary for adsorption reaction to occur, methoxy groups are quickly hydrolyzed before chemical adsorption on the silica surface. As a result, the molecules polymerize through their silanol groups. It is the resultant polymer that chemically binds the silica surface.

In view of intrinsic properties of both molecules and solvent solutions (Table 2) it was expected that class 1 SAMs would be generated by OTS and OTMS molecules, that class 2 SAMs would be the result of ODS and ODMS adsorption, and that HTMS would generate either class 1 or class 3 SAMs according to the solvent solution used. The particular properties of each class of substrates are described here after.

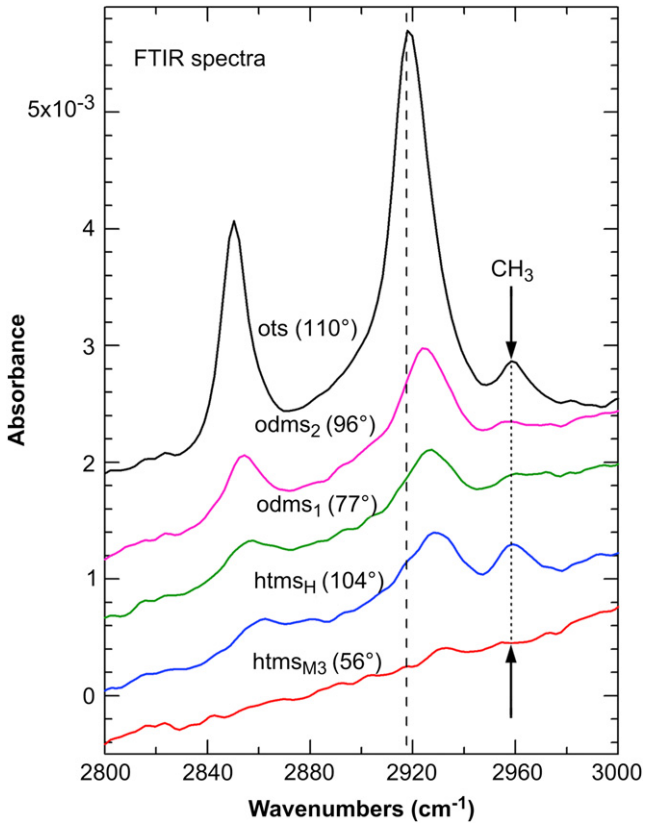

Fig. 3. FTIR spectra in the CH region of some substrates. FTIR spectra were background corrected by subtraction of a spectrum of the clean glass substrate (e.g., SAM-free). Spectra are offset for clarity. Peaks at ~2850 cm^{-1}, ~2920 cm^{-1}, and ~2955 cm^{-1} are respectively assigned to CH_2-ss, CH_2-as, and CH_3-as. Surface density of glass-bound alkylsiloxanes is reflected by the intensity of peaks, that depends on molecules alkyl chain length (for CH_2 peaks only) and on molecules organization inside the monolayers. This latter aspect is developed in the SFG spectra (Fig. 4) of the same substrates. The dashed line at ~2018 cm^{-1} represents close packed long chain SAM obtained for the ots substrate. Values in parentheses indicate the water contact angle on each substrate.

3.1. Quantitative analysis of substrates by FTIR spectroscopy

Modified substrates were probed by FTIR in the CH stretching region (Fig. 3). The "ideal" and well-studied monolayer made of OTS molecules is known to lead to a full coverage of the bare glass surface [36]. As expected, its FTIR spectrum in the CH region displayed the most intense peaks among all other SAMs studied. The CH peak intensity of odms substrates was lower than those of ots substrates, although the alkyl chain length is identical (Fig. 1). This indicates that $odms_1$ and $odms_2$ substrates have fewer molecules grafted per unit area. The higher intensity of CH_2 symmetric (CH_2-ss) and asymmetric (CH_2-as) stretches, in $odms_2$ compared to $odms_1$ substrate, can result from a higher quantity of adsorbed material, as supported by the higher contact angle value. In contrast to these surfaces, the $htms_{M3}$ substrates showed almost no visible CH peak, suggesting that the quantity of material grafted is under the detection limit of the FTIR spectrometer. Nevertheless, the presence of a non-negligible amount of CH groups at $htms_{M3}$ surface was suggested by the relatively high contact angle measured for water (56°) while a bare glass surface would undergo complete wetting (e.g., $\theta_{H2O} \approx 0°$).

The intensity of the CH peaks of $htms_H$ substrates was similar to that of odms substrates, although the HTMS molecule contains fewer CH_2 groups than ODMS (5 versus 17). This apparent discrepancy could result from monomers cross-linking, probable with HTMS, but impossible with ODMS. The binding of HTMS monomers to each other laterally would increase the number of adsorbed molecules per area. Surprisingly, the intensity of the CH_3 peak of $htms_H$ substrate was even greater than that of the ots substrate. AFM experiments revealed that the rms roughness of $htms_H$ substrate is remarkably higher (~1.4 nm) than that of the others substrates (~0.3 nm) which are supposed to display one single organic monolayer on the bare glass surface. These results suggest that the $htms_H$ modified surface is partially over covered by additional layers of HTMS molecules, possibly physisorbed on it. To determine whether the glass-bound layer of HTMS, and of the other molecules was coherently organized, a non-linear spectroscopic analysis was performed.

3.2. Qualitative analysis of surface-exposed CH groups organization by SFG

SFG spectra of ots and $htms_H$ (Fig. 4) displayed similar peaks, though the FTIR spectra of the two substrates were different (Fig. 3). The specificity of SFG to non-centrosymmetry ensures that the spectra emphasize the CH_3, as opposed to CH_2 groups present in an all-trans centrosymmetric environment. Both substrates formed ordered SAMs. This is evidenced from two well-defined peaks in the SSP spectra, at ~2875 cm^{-1} and ~2955 cm^{-1}, respectively assigned to the CH_3-ss and Fermi Resonance (FR) of CH_3 [37,38]. The absence, or the very small intensity, of CH_2 peaks (at ~2850 cm^{-1} and ~2925 cm^{-1}) further supported the formation of class 1, all-trans, SAMs (sketched in Fig. 2). In the PPP spectra, peaks at ~2965 cm^{-1} are assigned to CH_3-as [37,38]. Their intensity is consistent with the interpretation of the SSP spectra and in general with the formation of well-ordered SAMs.

SFG spectra of $odms_1$, $odms_2$ and $htms_{M3}$ indicated that the SAMs they formed were much more disordered compared to the class 1 SAMs discussed above. This is demonstrated in the PPP spectra by the absence of peak at ~2965 cm^{-1} (CH_3-as), or by very small and broad peaks that overlapped with peaks at ~2930 cm^{-1} (CH_2-as). The SSP spectra of these three substrates also confirmed the disordered organization of these surfaces. First, peaks at ~2875 cm^{-1} (CH_3-ss) were broader and/or smaller than that of ots and $htms_H$ substrates, second, CH_3-FR peaks (at 2955 cm^{-1}) overlapped with CH_2-as peaks (at ~2920–2930 cm^{-1}). And finally, the greater intensity of these latter peaks reflected gauche defects, a signature of surface-exposed CH_2 groups. Interestingly, the SSP spectra featured a CH_3-ss peak that is more intense for $odms_2$ than for $odms_1$ and $htms_{M3}$. Together with the contact angle value and FTIR spectra, this may indicate that the $odms_2$ substrate exhibited a few coherently arranged CH_3 groups, with a large number of ODMS molecules covalently bound to the glass surface. However, the $odms_2$ substrate does not appear to be as ordered as the class 1 SAMs.

Of all the substrates, $htms_{M3}$ substrate displayed the least intense peaks in the SFG spectra. This result could reflect the smaller amount of adsorbed molecules on glass, as indicated by both FTIR spectra and water contact angles (56° for $htms_{M3}$ versus 77° and 96° for $odms_1$ and $odms_2$, respectively). In particular, $htms_{M3}$ and $htms_H$ were characterised by distinctive spectra, demonstrating that one molecule can lead to wholly different surface properties according to the conditions of grafting in solution.

However, SFG spectra could not convincingly characterize the differences between class 2 SAMs ($odms_1$ and $odms_2$) and class 3 SAMs ($htms_{M3}$). Therefore, further analysis was required to discriminate class 2 and class 3 SAMs.

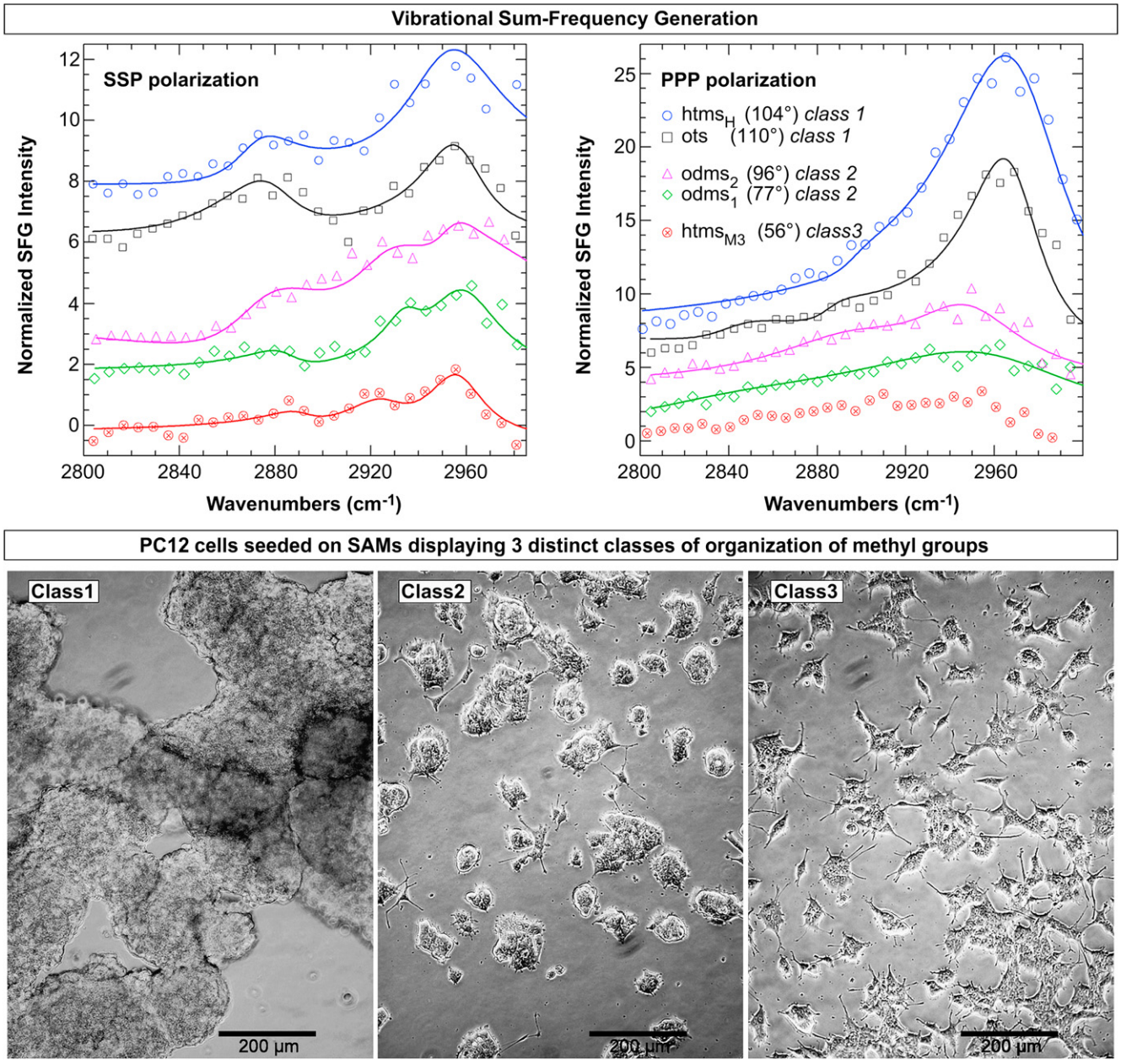

Fig. 4. SFG spectra of SAMs used as model culture substrates and PC12 cell adhesion and differentiation, without NGF treatment, on substrates 48 h after seeding. Top graphs feature SFG traces in the CH region for the substrates also analyzed by FTIR in Fig. 3. Spectra are offset for clarity. The polarization combination for SFG, visible and IR is S,S,P for left top graph, and P,P,P for right top graph. Clear surface organization (e.g., intense CH_3-group peaks and absence of CH_2 peaks) arises in class 1 substrates, compared to the others. Values in parentheses indicate the water contact angle on each substrate. PC12 cells have three distinct fates according to substrate class: no adhesion on class 1 SAM, relatively poor adhesion and neurite outgrowth on class 2 SAM, and good adhesion preceding neuronal differentiation on class 3 SAM. Observations were made 48 h after seeding with a contrast phase microscope.

3.3. SFE determination by contact angle measurements

Data obtained for contact angles, SFE, and roughness analysis, are recapitulated in Table 4. The overall surface tension γ_s of class 1 substrates ots and $htms_H$ was mostly composed of the dispersive component γ^d (Fig. 5), the polar contribution γ^p being close to zero. It suggests that very few OH groups were exposed, considering that γ^p is not generated by CH_3 groups. This result supports the close arrangement of monomers and its corollary: the complete coverage of the glass substrate. A similar result was obtained for the otms substrate, whose SFG spectra resemble those of class 1 SAMs (data not shown for clarity).

As expected, class 2 substrates $odms_1$, and ods (whose SFG spectra were similar to those of odms substrates—data not shown), displayed a more intense γ^p compared to class 1 substrates. This suggests the presence of surface-exposed OH groups, in agreement with the presence of disorganized alkyl chains and low intensity of FTIR peaks. The surface tension of an almost perfectly homogeneous CH_3 substrate is given by the γ_s of the ots substrate ($\sim$21.6 mN m^{-1}), close to the γ_c of the same substrate ($\sim$19.9 mN m^{-1}) obtained by a Zisman plot (Fig. 6). For a clean, bare glass substrate, estimations vary from 150 to 300 mN m^{-1} [39,40]. Consequently, it is of considerable importance to remark that, though the added contribution of γ^p to γ_s for class 2 substrates is

Table 4
Data collected from contact angle measurements and AFM. Contact angles (θ) were measured using water, glycerol (GL), formamide (FA), tetradecane (TD), and n-hexadecane (HD) as test liquids. Uncertainty on a measured contact angle was statistically estimated to less than 1°. $\Delta\theta$ is the difference between advancing and receding contact angles of water. The critical surface tension (γ_c, ±1.5 mN m^{-1}) was determined from Zisman plots, displayed in Fig. 6, using contact angles of all test liquids. The polar (γ_s^p) and dispersive (γ_s^d) components of the overall surface tension (γ_s, ±1.0 mN m^{-1}) of the solid substrates were determined from the water and n-hexadecane contact angles. Values of the root-mean-square roughness (±0.1 nm) are the mean of three independent measurements.

		ots	ods	otms	$odms_1$	$odms_2$	$htms_{M1}$	$htms_{M3}$	$htms_H$	$htms_{Hx}$
θ_{H2O}	deg	110	82	105	77	96	38	56	104	98
θ_{GL}	deg	99	77	92	68	81	34	51	91	87
θ_{FA}	deg	90	68	89	58	75	31	45	83	83
θ_{HD}	deg	40	31	29	13	24	6	11	34	21
θ_{TD}	deg	35	7	15	–	–	–	–	26	12
γ_c	mN m^{-1}	19.9	23	23.7	26.7	24	26.5	25.7	22.7	24.9
γ_s^d	mN m^{-1}	21.5	23.7	24.2	26.8	25.2	27.3	27	23.1	25.8
γ_s^p	mN m^{-1}	0.1	6.9	0.3	8.2	1.6	32.6	20.9	0.6	1.2
γ_s	mN m^{-1}	21.6	30.6	24.5	35	26.8	59.9	47.9	23.6	26.9
rms	nm	0.3	0.3	0.3	0.3	0.3	0.9	0.3	1.4	0.4
$\Delta\theta$	deg	12	17	12	15	11	32	22	30	12

relatively small (1.6 mN m^{-1} ≤ γ^p ≤ 8.2 mN m^{-1}), locally the surface energy gradients can reach much higher values (20 mN m^{-1} ≤ γ_c ≤ 150 mN m^{-1}).

Class 3 substrates, e.g., $htms_{M1}$ and $htms_{M3}$, displayed higher γ^p (≥20.9 mN m^{-1}) than both class 1 (≤0.6 mN m^{-1}) and class 2 substrates (≤8.2 mN m^{-1}). The smaller γ^p of $htms_{M3}$ (~20.9 mN m^{-1}) compared to that of $htms_{M1}$ (~32.6 mN m^{-1}) indicates that more HTMS molecules adsorbed on glass in $htms_{M3}$. As $htms_{M3}$ was very smooth (rms ≈ 0.3 nm), it appears that HTMS may have bound to the majority of substrate silanol sites still available for adsorption. Moreover, θ_{H2O} could not be further increased by lengthening the time of adsorption in the methanol/water solution, supporting the conclusion of HTMS optimal adsorption in these conditions. Nevertheless, the quantity of adsorbed HTMS was relatively small, as evidenced by the absence of peaks in the $htms_{M3}$ FTIR spectrum (Fig. 3). Therefore the greater part of the γ^d contribution to the γ_s of $htms_{M3}$ was provided by OH groups. As a result $htms_M$ substrates exhibited a chemical pattern that was mostly glass-like, with a heterogeneous distribution of CH_3 groups. Conversely, class 2 SAMs mostly exhibited CH_3 groups, together with more ($odms_1$ and ods) or less ($odms_2$) scattered OH groups.

$odms_2$ and $htms_{Hx}$ are particular substrates. $odms_2$ substrate concentrated more molecules than $odms_1$, as evidenced by the FTIR spectra, and its γ_s components resembled those of class 1 substrates, whose γ^p was close to zero. However, the γ^p of $odms_2$ (~1.6 mN m^{-1}) was higher than the γ^p of class 1 substrates (γ^p < 0.6 mN m^{-1}). Moreover, the SFG spectra evidenced the disordered organization of CH groups in $odms_2$ substrate. Therefore $odms_2$ cannot be considered as sharing properties of class 1 substrates. $Htms_{Hx}$ substrate was made by agitating the solution in order to prevent HTMS molecules from over covering the substrate (rms ≈ 0.3 nm for $htms_{Hx}$ versus ~1.4 nm for $htms_H$). However, this process also apparently slowed the reaction kinetics, resulting in an incomplete monolayer. This is evidenced by θ_{H2O} on $htms_{Hx}$ (98°), smaller than θ_{H2O} on $htms_H$ (104°). This suggests that the $htms_{Hx}$ substrate exhibited some OH groups that contributed to a small γ^p (~1.2 mN m^{-1}), and though originally forming a class 1 SAM, it did not share the same surface energy distribution. The SFG spectra of the $otms_x$ substrate featured similar traces than those of class 2 substrates (data not shown for clarity), and θ_{H2O} was also smaller on $otms_x$ (100°) than on otms (105°). Consequently, $htms_{Hx}$ and $otms_x$ substrates shared the properties of class 2 substrates.

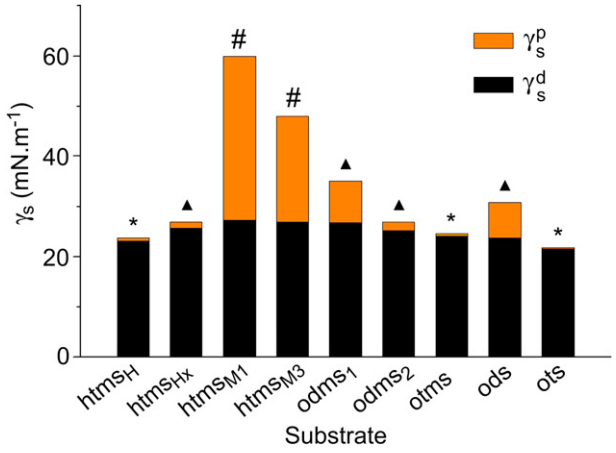

Fig. 5. SFE components γ^d and γ^p of solid substrates. γ^d and γ^p were calculated through the measurements of water and n-hexadecane contact angles, displayed in Table 4, using the Owens–Wendt theoretical model. Notes indicate PC12 cell fate on substrates 48 h after seeding: either the cells did not adhere (*), or they adhered, regrouped in clusters, and initiate few neurites (▲), or the adhesion was enhanced and the cells generated many neurites (#).

The values of γ_c, determined by Zisman plots (Fig. 6 and Table 4), were in agreement with previous results. γ_c can be assimilated to γ^d of solid substrates [41], and the gap between γ_c and γ^d never exceeded 1.6 mN m^{-1} (Table 4). In addition γ_c was always smaller in "ordered" substrates than in "disordered" substrates made of similar molecules. For instance, following relations were obtained: γ_c (ots) < γ_c (ods), γ_c (otms) < γ_c ($odms_2$) < γ_c ($odms_1$), and γ_c ($htms_H$) < γ_c ($htms_{Hx}$) < γ_c ($htms_{M3}$) < γ_c ($htms_{M1}$). More generally, γ_c values were in the same range (19.9 mN m^{-1} < γ_c < 26.7 mN m^{-1}), thus supporting the idea that substrates are rather comparable in terms of nanoscale SFE distribution than in terms of overall surface tension.

The difference between advancing and receding contact angles of water (noted $\Delta\theta$) is a good control to evaluate physical roughness and/or chemical heterogeneity of surfaces [42–44]. $\Delta\theta$ values were in good agreement with both rms roughness and SFE distribution. Among smooth substrates whose rms roughness was ~0.3 nm, those generating the smallest γ^p also generated the smallest $\Delta\theta$ (Table 4). On ods and $odms_1$ substrates, whose γ^p was higher than that of ots, otms, $odms_2$, $htms_H$ and $htms_{Hx}$ substrates (Fig. 5 and Table 4), $\Delta\theta$ was higher as well (~15–17° versus ~12°). It was further higher on $htms_{M3}$ ($\Delta\theta$ ≈ 22°) whose surface tension is locally more heterogeneous. Finally, the largest values ($\Delta\theta$ ≈ 30°) were obtained for substrates exhibiting high roughness: $htms_{M1}$ (rms ≈ 0.9 nm) and $htms_H$ (rms ≈ 1.4 nm).

3.4. PC12 cell adhesion and differentiation on modified substrates

When seeded on a clean, bare glass substrate, PC12 cells poorly adhered and tend to detach by 48 h. On well-ordered SAMs, such

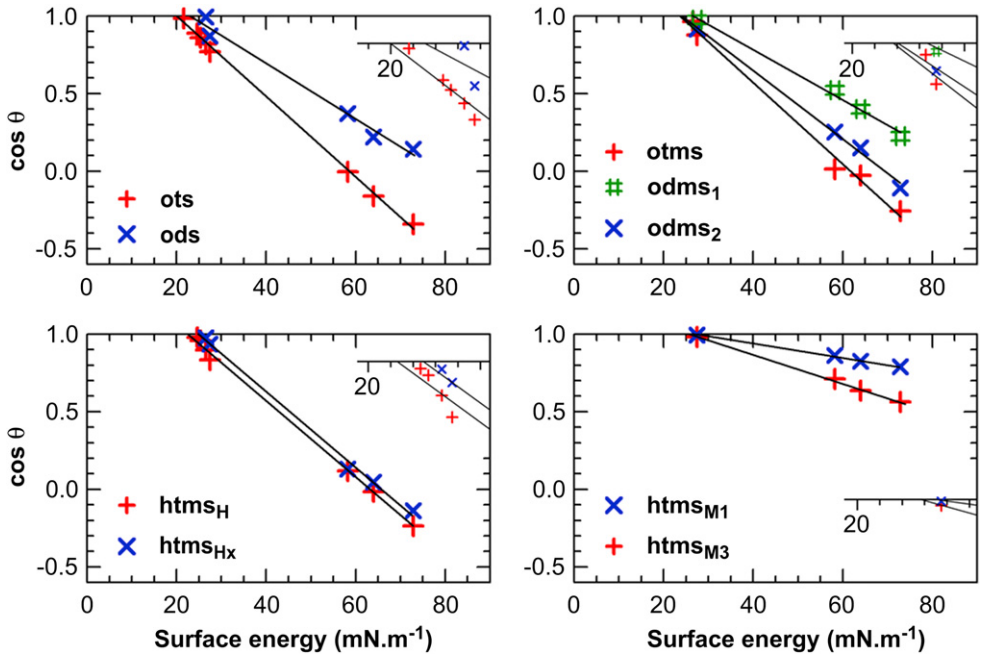

Fig. 6. Zisman plots used to determine the critical surface tension (γ_c) of solid substrates. γ_c values were read where the line fits intersect $\cos\theta = 1$ (numerical values are displayed in Table 4). For each substrates the line fit resulted in $R^2 > 0.99$, except for the ods substrate ($R^2 > 0.985$). Insets: enlargement of the area where the line fits intersect $\cos\theta = 1$ (e.g., γ_c).

as class 1 substrates, PC12 cells did not adhere at all, and clusters of cells were observed that floated over the surface (Fig. 4). This reveals the poor affinity of PC12 cells for substrates exclusively composed of OH groups, or of CH_3 groups. On the contrary, cells did adhere on class 2 and on class 3 SAMs, as well as on incomplete class 1 SAMs. Therefore, it appears that adhesion is favored as soon as some disorder is introduced in the surface arrangement of CH_3 groups. We further hypothesize that is because OH groups, pointing out from the surface, are accessible to the cells. In addition, PC12 cells initiated more neurites (Figs. 4 and 7) on class 3 SAMs (more than 50 mm^{-2}) than on class 2 SAMs or on incomplete class 1 SAMs (less than 20 mm^{-2}). All in all, it appears that, the more locally heterogeneous is the surface, the more PC12 cells generate neurites. These results are in complete agreement with those of our previous study [5], and provide further evidence that surface disorder, and thus local gradients in surface energy, can trigger neuritogenesis in PC12 cells albeit the absence of NGF treatment.

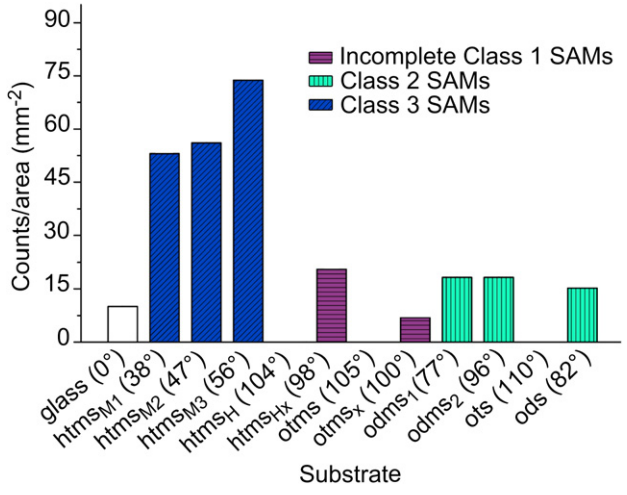

Fig. 7. Propensity of PC12 cells to initiate neurite outgrowth without NGF treatment, according to the substrate, 48 h after seeding. Several pictures of cells were taken and the number of grown neurites ($L > 25$ μm) was counted on each substrate. The data are from one experiment representative of at least three independent measurements. They reflect typical differences between substrate classes. On class 1 SAMs, cells did not adhere, and thus did not initiate any neuritis. Conversely, on class 2 SAMs and incomplete class 1 SAMs, cells adhered and initiate few neurites. On class 3 SAMs, adhesion was enhanced and cells generated more neurites. The values in parentheses indicate the water contact angle on each substrate.

Our results also indicate that PC12 cells were not highly sensitive to the nanoroughness of our substrates. Cell adhesion and neuritogenesis were similar in ots (rms ≈ 0.3 nm) and in $htms_H$ (~1.4 nm). They were also similar in $htms_{M1}$ (~0.9 nm) and in $htms_{M3}$ (~0.3 nm) substrates (Fig. 7). A potential explanation to this result is that the nanoroughness of our substrates is too low to have a critical influence on PC12 cell adhesion and differentiation. In addition, neither the hydrophobicity degree, nor the surface concentration of methyl groups seemed to profoundly affect PC12 cell behavior. The propensity of cells to adhere and differentiate were not significantly different in class 2 SAMs $odms_1$ ($\theta_{H2O} = 77°$) and $odms_2$ (96°), or in class 1 SAMs ots (110°) and $htms_H$ (104°), while differences were obvious between class 2 SAM $odms_1$ (77°) and class 3 SAM $htms_{M3}$ (56°), or between class 1 SAM $htms_H$ (104°) and incomplete class 1 SAM $htms_{Hx}$ (98°). As a result the chemical heterogeneity, that is the alternation between CH_3 and OH groups at the nanoscale level, seemed to be the determinant factor in generating the surface energy gradients that the cells were able to sense.

The dimension for which these gradients may become effective is still questionable, since the gradients can theoretically emerge out from the surface as soon as a few single OH groups become accessible to the cells. However, actin-based processes such as lamellipodial and filopodial activity can probe the substrate at a dimension of ~150 μm [5,45], which may indicate the dimensional range for which the gradients become effective and thus sensed by the cells. Therefore, a potential explanation for this sensing might reside in the translation of the local gradients through lamellipodia and filopodia that can be mediated by external factors, such as calcium transients [46,47].

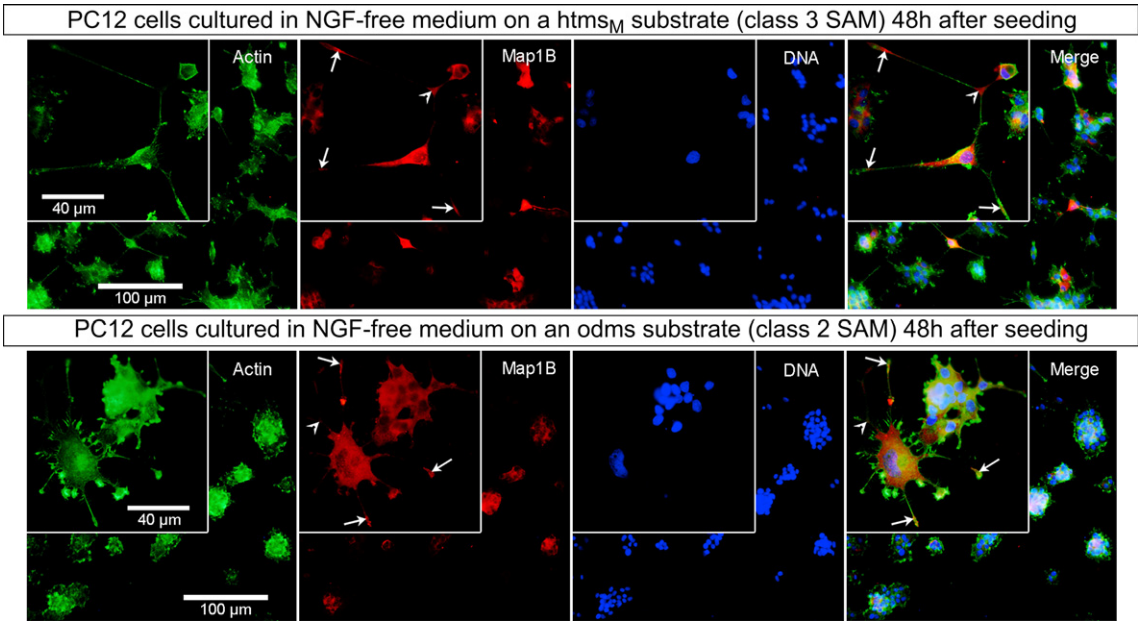

Fig. 8. MAP1B expression and localization in PC12 cells cultured on htms$_M$ and odms substrates, without NGF treatment. MAP1B signal is stronger in isolated cells than in clustered cells. More cells display a strong signal and cells are more often apart on an htms$_M$ substrate than on an odms one, where cells rather tend to group in clusters. Inset boxes: arrows point at higher local concentrations of MAP1B upstream of the growth cones (plain arrows) and at branching/turning points (broken arrows).

Though PC12 cells adhered on moderately disordered class 2 SAMs, they tended to gather in clusters (Figs. 4 and 8), suggesting that these substrates were not optimal, and that cell–cell interactions were favored over cell–substrate adhesive strengths, a typical feature of PC12 cells [48]. Conversely, on highly disordered class 3 SAMs, cells scattered across the surface, with single cells tended to spread (Figs. 4 and 8). This indicates a strong adhesion to the substrate, together with cells showing signs of polarization, what may prefigure neuritis extension [49]. This can be correlated with the higher γ_s of class 3 substrates ($\geq$47.9 mN m^{-1}) over class 2 substrates ($\leq$35 mN m^{-1}), in agreement with the dependence of cell-aggregates spreading rate over the substrate adhesivity, that was reported in Ref. [50].

A criterion to evaluate neuronal differentiation is a high level of expression of neuronal markers proteins like MAP1B. MAP1B is a neuron-specific protein involved in microtubule assembly [51]. NGF treatment stimulates MAP1B expression together with PC12 cell differentiation [52]. As expected, high levels of fluorescence reflecting MAP1B concentration was detected in cells that underwent neurite outgrowth on class 3 and on class 2 SAMs, typically in isolated cells or at the periphery of cell clusters, rather than in cells trapped in clusters (Fig. 8). Better adhesiveness allowed more cells to remain apart, not to cluster, on class 3 substrates, whose ability to promote adhesion and to trigger neuronal differentiation of PC12 cells was thereby stronger than that of class 2 substrates. In view of these results, it can be suggested that PC12 cells would adhere but not differentiate if they were seeded on an NH_2-terminated class 1 SAM, as observed on smooth substrates such as bare glass coated with poly-L-lysine or poly-L-ornithine [5].

MAP1B localization in differentiated cells was similar whether PC12 cells were seeded on class 2 or on class 3 substrates (Fig. 8; inset boxes). MAP1B was mostly displayed in the cell soma. Interestingly, MAP1B was also displayed upstream of growth cones (Fig. 8; plain arrows), and at branching/turning points of the neurites (Fig. 8; broken arrows), that is where microtubules are highly dynamic. These results indicate that cell–substrate interactions can mimic NGF effects, leading PC12 cells to start neuritogenesis.

The fact that it only took 48 h for neurites to extend up to ~100 µm, compared to 4–6 days in our previous study [5], might be related to the reduced volume of medium (V = 2 mL to V = 335 µL) used for cell seeding in these experiments. Considering that cells might respond to surface energy gradients, by secreting neurotrophic factors, like NGF, their concentration in the cell environment would be higher in this experimental set. Higher concentrations of NGF, for example, are expected to facilitate the activation of signalling pathways leading to neurite outgrowth.

4. Conclusions

In this study, we manufactured culture substrates by distinct chemical treatments of bare glass surfaces in order to obtain an acute control of substrate physical and chemical cues that may be sensed by the cells. We introduced a new perspective on self-assembled-monolayers (SAMs) used as a culture substrate, by ranking them in three distinct classes, including highly ordered surface (class 1), moderately ordered surface (class 2), and highly disordered surface (class 3). Highly surface specific techniques have been used to characterize the substrates. In addition to commonly used FTIR and AFM, the analysis combined SFG, a non-linear optical technique that unveils the surface ordering, with wetting experiments, using the Owens–Wendt model that distinguishes dispersive and polar components of the surface free energy. Taken together, the results harmoniously combined to ascribe to each substrate class a distinct nanostructured organization that generated a specific surface free-energy distribution. Thence, we identified what is the most important parameter involved in generating the SFE gradients that the cells were able to sense. Of all the factors analyzed, including surface nanoroughness, wettability, chemical affinity, terminal-groups concentration, and nanoscale chemical heterogeneities, we demonstrate that, in our experiments, it is nanoscale chemical heterogeneities that have a critical influence on both the adhesion and the differentiation of PC12 cells. Moreover, we show that PC12 cells can reach a fully stable state of differentiation by 48 h of culture on rigid model surfaces (class 3 SAMs of

alkylsiloxanes on glass), without nerve growth factor treatment. Earlier experimental data demonstrating the influence of substrate factors, such as mechanical, spatial and chemical cues, on neuronal cell functions, would gain in being reappraised in light of this new criterion (e.g., substrate nanoscale chemical heterogeneities) and, in turn, future experiments will have to challenge it. It is reasonable to assume that other systems, in addition to PC12 cells, such as primary neurons or astrocytes, may be dramatically affected by nanoscale surface organization. Therefore, future design of biomaterials may integrate local gradients in surface free energy as a mean to enhance regeneration of hippocampal or cortical neurons for instance. In addition, future experiments should investigate the mediators of the nanoscale SFE gradients. In particular, it should be determined whether PC12 cells can respond to these substrate physical cues directly or through components of the culture medium such as calcium and serum proteins.

Acknowledgements

We thank Dr. Sylvain Gabriele for critical reading of the manuscript.

The Descartes group acknowledges the support of the French Ministry of Research, the University of Paris Diderot, the IFR95, and of the University of Paris Descartes. The Temple group acknowledges the support of the NSF.

Appendix

Figures with essential colour discrimination. Most of the figures in this article have parts that are difficult to interpret in black and white. The full colour images can be found in the on-line version, at doi:10.1016/j.biomaterials.2010.01.099.

References

[1] Letourneau PC. Cell-to-substratum adhesion and guidance of axonal elongation. Dev Biol 1975;44:92–101.
[2] Letourneau PC. Possible roles for cell-to-substratum adhesion in neuronal morphogenesis. Dev Biol 1975;44:77–91.
[3] Suter DM, Forscher P. Substrate–cytoskeletal coupling as a mechanism for the regulation of growth cone motility and guidance. J Neurobiol 2000;44:97–113.
[4] Murnane AC, Brown K, Keith CH. Preferential initiation of PC12 neurites in directions of changing substrate adhesivity. J Neurosci Res 2002;67:321–8.
[5] Lamour G, Journiac N, Souès S, Bonneau S, Nassoy P, et al. Influence of surface energy distribution on neuritogenesis. Colloids Surf B Biointerfaces 2009;72:208–18.
[6] Fan YW, Cui FZ, Hou SP, Xu QY, Chen LN, et al. Culture of neural cells on silicon wafers with nano-scale surface topograph. J Neurosci Methods 2002;120:17–23.
[7] Badami AS, Kreke MR, Thompson MS, Riffle JS, Goldstein AS. Effect of fiber diameter on spreading, proliferation, and differentiation of osteoblastic cells on electrospun poly(lactic acid) substrates. Biomaterials 2006;27:596–606.
[8] Staii C, Viesselmann C, Ballweg J, Shi L, Liu G, et al. Positioning and guidance of neurons on gold surfaces by directed assembly of proteins using atomic force microscopy. Biomaterials 2009;30:3397–404.
[9] Xiong Y, Lee AC, Suter DM, Lee GU. Topography and nanomechanics of live neuronal growth cones analyzed by atomic force microscopy. Biophys J 2009;96:5060–72.
[10] Stenger DA, Pike CJ, Hickman JJ, Cotman CW. Surface determinants of neuronal survival and growth on self-assembled monolayers in culture. Brain Res 1993;630:136–47.
[11] Lee MH, Brass DA, Morris R, Composto RJ, Ducheyne P. The effect of non-specific interactions on cellular adhesion using model surfaces. Biomaterials 2005;26:1721–30.
[12] Ren Y, Zhang H, Huang H, Wang X, Zhou Z, et al. In vitro behavior of neural stem cells in response to different chemical functional groups. Biomaterials 2009;30:1036–44.
[13] Saha K, Keung AJ, Irwin EF, Li Y, Little L, et al. Substrate modulus directs neural stem cell behavior. Biophys J 2008;95:4426–38.
[14] Teixeira AI, Ilkhanizadeh S, Wigenius JA, Duckworth JK, Inganas O, et al. The promotion of neuronal maturation on soft substrates. Biomaterials 2009;30:4567–72.
[15] Janmey PA, Winer JP, Murray ME, Wen Q. The hard life of soft cells. Cell Motil Cytoskeleton 2009;66:597–605.
[16] Leipzig ND, Shoichet MS. The effect of substrate stiffness on adult neural stem cell behavior. Biomaterials 2009;30:6867–78.
[17] Flanagan LA, Ju YE, Marg B, Osterfield M, Janmey PA. Neurite branching on deformable substrates. Neuroreport 2002;13:2411–5.
[18] Schwarz US, Bischofs IB. Physical determinants of cell organization in soft media. Med Eng Phys 2005;27:763–72.
[19] Senaratne W, Andruzzi L, Ober CK. Self-assembled monolayers and polymer brushes in biotechnology: current applications and future perspectives. Biomacromolecules 2005;6:2427–48.
[20] Barrias CC, Martins MCL, Almeida-Porada G, Barbosa MA, Granja PL. The correlation between the adsorption of adhesive proteins and cell behaviour on hydroxyl-methyl mixed self-assembled monolayers. Biomaterials 2009;30:307–16.
[21] Kleinfeld D, Kahler KH, Hockberger PE. Controlled outgrowth of dissociated neurons on patterned substrates. J Neurosci 1988;8:4098–120.
[22] Kapur R, Rudolph AS. Cellular and cytoskeleton morphology and strength of adhesion of cells on self-assembled monolayers of organosilanes. Exp Cell Res 1998;244:275–85.
[23] Sukenik CN, Balachander N, Culp LA, Lewandowska K, Merritt K. Modulation of cell-adhesion by modification of titanium surfaces with covalently attached self-assembled monolayers. J Biomed Mater Res 1990;24:1307–23.
[24] Wehrman T, He X, Raab B, Dukipatti A, Blau H, et al. Structural and mechanistic insights into nerve growth factor interactions with the TrkA and p75 receptors. Neuron 2007;53:25–38.
[25] Mischel PS, Umbach JA, Eskandari S, Smith SG, Gundersen CB, et al. Nerve growth factor signals via preexisting TrkA receptor oligomers. Biophys J 2002;83:968–76.
[26] Greene LA, Tischler AS. Establishment of a noradrenergic clonal line of rat adrenal pheochromocytoma cells which respond to nerve growth factor. Proc Natl Acad Sci U S A 1976;73:2424–8.
[27] Fujii DK, Massoglia SL, Savion N, Gospodarowicz D. Neurite outgrowth and protein synthesis by PC12 cells as a function of substratum and nerve growth factor. J Neurosci 1982;2:1157–75.
[28] Wujek JR, Akeson RA. Extracellular matrix derived from astrocytes stimulates neuritic outgrowth from PC12 cells in vitro. Brain Res 1987;431:87–97.
[29] Arkles B. Tailoring surfaces with silanes. Chemtech 1977;7:766–78.
[30] Shen YR. Sum-frequency generation. In: The principles of nonlinear optics. New York: Wiley-Interscience; 1984. pp. 67–85.
[31] Eftekhari-Bafrooei A, Borguet E. Effect of surface charge on the vibrational dynamics of interfacial water. J Am Chem Soc 2009;131:12034–5.
[32] Owens DK, Wendt RC. Estimation of surface free energy of polymers. J Appl Polym Sci 1969;13:1741–7.
[33] Kwok DY, Li D, Neumann AW. Evaluation of the Lifshitz Van-der-Waals acid–base approach to determine interfacial-tensions. Langmuir 1994;10:1323–8.
[34] Zisman WA. Contact angle, wettability and adhesion. Adv Chem Ser 1964;43:1–51.
[35] Good RJ, Girifalco LA. A theory for estimation of surface and interfacial energies.3. Estimation of surface energies of solids from contact angle data. J Phys Chem 1960;64:561–5.
[36] Ulman A. Formation and structure of self-assembled monolayers. Chem Rev 1996;96:1533–54.
[37] Porter MD, Bright TB, Allara DL, Chidsey CED. Spontaneously organized molecular assemblies .4. Structural characterization of normal-alkyl thiol monolayers on gold by optical ellipsometry, infrared-spectroscopy, and electrochemistry. J Am Chem Soc 1987;109:3559–68.
[38] Guyotsionnest P, Superfine R, Hunt JH, Shen YR. Vibrational spectroscopy of a silane monolayer at air solid and liquid solid interfaces using sum-frequency generation. Chem Phys Lett 1988;144:1–5.
[39] Fisher JC. The fracture of liquids. J Appl Phys 1948;19:1062–7.
[40] Degennes PG, Brochard-Wyart F, Quéré D. Capillarité: Interfaces mobiles. In: Gouttes, bulles, perles et ondes. Paris: Belin; 2005. pp. 11–37.
[41] Adamson AW, Gast AP. The solid–liquid interface-contact angle. In: Physical chemistry of surfaces. 6th ed. New York: Wiley-Interscience; 1997. pp. 347–89.
[42] Degennes PG. Wetting – statics and dynamics. Rev Mod Phys 1985;57:827–63.
[43] Chow TS. Wetting of rough surfaces. J Phys Condens Matter 1998;10:L445–51.
[44] Zografi G, Tam SS. Wettability of pharmaceutical solids – estimates of solid-surface polarity. J Pharm Sci 1976;65:1145–9.
[45] Mogilner A, Rubinstein B. The physics of filopodial protrusion. Biophys J 2005;89:782–95.
[46] Gomez TM, Robles E, Poo M, Spitzer NC. Filopodial calcium transients promote substrate-dependent growth cone turning. Science 2001;291:1983–7.
[47] Veksler A, Gov NS. Calcium-actin waves and oscillations of cellular membranes. Biophys J 2009;97:1558–68.
[48] Greene LA, Aletta JM, Rukenstein A, Green SH. PC12 pheochromocytoma cells: culture, nerve growth factor treatment, and experimental exploitation. Methods Enzymol 1987;147:207–16.
[49] Matta LL, Aranda-Espinoza H. Neuronal systems & modeling; strong adhesion identifies potential neurite extension and polarization sites in PC12 cells. Biophys J 2008;94:1055–7.
[50] Ryan PL, Foty RA, Kohn J, Steinberg MS. Tissue spreading on implantable substrates is a competitive outcome of cell-cell vs. cell-substratum adhesivity. Proc Natl Acad Sci USA 2001;98:4323–7.
[51] Gordonweeks PR. Growth cones – the mechanism of neurite advance. Bio-Essays 1991;13:235–9.
[52] Drubin DG, Feinstein SC, Shooter EM, Kirschner MW. Nerve growth factor-induced neurite outgrowth in PC12 cells involves the coordinate induction of microtubule assembly and assembly-promoting factors. J Cell Biol 1985;101:1799–807.